UC Irvine

UC Irvine Previously Published Works

Title

Extracellular Vesicle–Derived miR-124 Resolves Radiation-Induced Brain Injury

Permalink

https://escholarship.org/uc/item/3vw8d7zs

Journal

Cancer Research, 80(19)

ISSN

0008-5472

Authors

Leavitt, Ron J
Acharya, Munjal M
Baulch, Janet E
et al.

Publication Date

2020-10-01

DOI

10.1158/0008-5472.can-20-1599

Peer reviewed

eScholarship.org Powered by the California Digital Library
University of California

Published OnlineFirst August 19, 2020; DOI: 10.1158/0008-5472.CAN-20-1599

Extracellular Vesicle–Derived miR-124 Resolves Radiation-Induced Brain Injury

Ron J. Leavitt, Munjal M. Acharya, Janet E. Baulch, and Charles L. Limoli

ABSTRACT

Radiation-induced cognitive dysfunction (RICD) is a progressive and debilitating health issue facing patients following cranial radiotherapy to control central nervous system cancers. There has been some success treating RICD in rodents using human neural stem cell (hNSC) transplantation, but the procedure is invasive, requires immunosuppression, and could cause other complications such as teratoma formation. Extracellular vesicles (EV) are nanoscale membrane-bound structures that contain biological contents including mRNA, miRNA, proteins, and lipids that can be readily isolated from conditioned culture media. It has been previously shown that hNSC-derived EV resolves RICD following cranial irradiation using an immunocompromised rodent model. Here, we use immunocompetent wild-type mice to show that hNSC-derived EV treatment administered either intravenously via retro-orbital vein injection or via intracranial transplantation can ameliorate cognitive deficits following 9 Gy head-only irradiation. Cognitive function assessed on the novel place recognition, novel object recognition, and temporal order tasks was not only improved at early (5 weeks) but also at delayed (6 months) postirradiation times with just a single EV treatment. Improved behavioral outcomes were also associated with reduced neuroinflammation as measured by a reduction in activated microglia. To identify the mechanism of action, analysis of EV cargo implicated miRNA (miR-124) as a potential candidate in the mitigation of RICD. Furthermore, viral vector–mediated overexpression of miR-124 in the irradiated brain ameliorated RICD and reduced microglial activation. Our findings demonstrate for the first time that systemic administration of hNSC-derived EV abrogates RICD and neuroinflammation in cranially irradiated wild-type rodents through a mechanism involving miR-124.

Significance: Radiation-induced neurocognitive decrements in immunocompetent mice can be resolved by systemic delivery of hNSC-derived EVs involving a mechanism dependent on expression of miR-124.

Introduction

Persistent, progressive, and debilitating cognitive decline following cranial radiotherapy is a growing concern as survivorship increases with more efficacious brain tumor treatments. Treatment plans for brain and central nervous system (CNS) metastases generally consist of surgical resection followed by radiotherapy and chemotherapy, collectively known as combination therapy (1). Systemic or focal radiotherapy can elicit a range of associated pathologies in the brain including changes to the vascular bed, neurogenesis, mature and immature neuronal structure damage, inflammatory responses, and expression of neurotrophic factors (2). As a result, the majority of survivors who received cranial radiotherapy report a range of degenerative sequelae, including difficulties in learning and memory, attention, executive function, decision-making, and mood, that typically manifest late after treatment and progressively deteriorate over time (3). In pediatric cases, resultant cognitive impairments that significantly reduce quality of life are particularly problematic because long-term survival rates are high (4–6). Despite improvements in therapeutic outcome, radiation-induced cognitive dysfunction (RICD) remains a critical unmet medical need that adversely affects an ever-growing patient base without any therapeutic recourse.

Previous work from our laboratory has pioneered the use of transplanted multi- and pluripotent human stem cells to ameliorate a variety of radiation-induced normal tissue injuries including neurocognitive decline. Our past data have shown that intracranial transplantation of human neural stem cells (hNSC) between 2 and 30 days following irradiation ameliorated cognitive deficits, reduced neuroinflammation, and preserved neuronal architecture in athymic nude rats (7–10). While stem cell transplantation strategies remain a promising therapeutic approach, caveats for translating this technology to the clinic include the requirement for cranial surgical procedures, the need for immunosuppression (11), and the risk of teratoma formation (12, 13). To address these caveats, we subsequently demonstrated that intrahippocampal transplantation using hNSC-derived extracellular vesicles (EV) was equally as efficacious in ameliorating the effects of cranial irradiation in immunocompromised athymic nude rats (14, 15). In these studies, grafted EVs were found to mitigate a range of radiation-induced pathologies in the brain, including cognitive dysfunction, neuroinflammation, and reductions in the structural complexity of neurons and synaptic integrity. While it was striking that EVs were functionally equivalent to the transplanted stem cells in resolving RICD, literature did suggest that the secretome, rather than cell replacement, could be the dominant therapeutic mechanism driving the beneficial outcomes following stem cell transplantation (16–20).

EV is a broad term used to describe a variety of nano-scale membrane-bound structures often referred to as exosomes or microvesicles, depending on size and mechanism of synthesis, that are secreted by cells and can participate in paracrine and endocrine

Department of Radiation Oncology, University of California, Irvine, Irvine, California.

Note: Supplementary data for this article are available at Cancer Research Online (http://cancerres.aacrjournals.org/).

Corresponding Authors: Charles L. Limoli, University of California, Irvine, Medical Sciences I, Room B-146B, Irvine, CA 92697-2695. Phone: 949-824-3053; E-mail: climoli@uci.edu; and Janet E. Baulch, Phone: 949-824-7396; E-mail: jbaulch@uci.edu

Cancer Res 2020;80:4266–77

doi: 10.1158/0008-5472.CAN-20-1599

©2020 American Association for Cancer Research.

Downloaded from cancerres.aacrjournals.org on December 28, 2020. © 2020 American Association for Cancer Research.

Published OnlineFirst August 19, 2020; DOI: 10.1158/0008-5472.CAN-20-1599

signaling (21). Contents of EVs include lipids, nucleic acids (e.g., genomic DNA, miRNAs, and mRNAs), proteins, and in some cases mitochondria (22). On the basis of the evidence available to date, miRNAs are considered to be critical functional cargo within EV given that a single miRNA is capable of impacting multiple gene targets and signaling pathways (23). EVs are recognized as specialized long distance mediators of intercellular communication, and the small size and lipid-heavy composition of the particles facilitate their translocation across the blood–brain barrier (24, 25), ideally suiting them to deliver their bioactive cargo into select target cell populations in the brain. The substitution of EVs for stem cells to resolve RICD has several distinct advantages including: (i) eliminating the risk of teratoma formation, (ii) minimizing complications associated with immunogenicity (26), and (iii) providing a more amenable systemic route of administration that negates the need for invasive surgical procedures. In this study, we have treated immunocompetent, cranially irradiated mice with hNSC-derived EVs to demonstrate proof of principle for the potential translational benefits of EV treatment as a safe and noninvasive strategy for long-term amelioration of RICD. We further report that analysis of EV miRNA cargo identified miR-124, a candidate molecule that we validate to be capable of mitigating RICD and neuroinflammation when overexpressed *in vivo* following cranial irradiation.

Materials and Methods

hNSC culture and EV isolation and characterization

The use of hNSC was approved by the Institutional Human Stem Cell Research Oversight Committee. The validation, expansion, and characterization of hNSCs (ENStem-A; EMD Millipore) followed previously published procedures (7, 27). EVs were isolated and purified from conditioned hNSC culture medium by ultracentrifugation (28) and characterized using a Nano-particle Analyzer (ZetaView PMX 110). The ENStem conditioned media yielded 4.19×10^8 EVs with a size distribution of 118.6 ± 59.1 nm (diameter). These purified EVs were used for all of the experiments described.

Animal irradiation and transplant surgeries

All animal procedures described in this study were in accordance with NIH guidelines and approved by the University of California Irvine Institutional Animal Care and Use Committee. Four- to 5-month-old wild-type male mice (C57BL/6, The Jackson Laboratory) were maintained in standard housing conditions ($20°C \pm 1°C$; $70\% \pm 10\%$ humidity; and 12:12-hour light and dark cycle) and provided *ad libitum* access to food (Envigo Teklad 2020x) and water. For all studies, mice were immobilized and subjected to 9 Gy cranial irradiation using a ^{137}Cs γ irradiator at a dose rate of 2.07 Gy/minute (Mark I, J.L. Sheppard and Associates). Concurrent control mice were immobilized and placed into the irradiator for the same length of restraint and exposure time as that required to deliver the 9 Gy dose. Experimental design is shown in a schematic (**Fig. 1A**)

EV cohort

A single cohort of mice was randomly assigned to the following four experimental groups (100 mice total, $n = 24$–26/group): control (sham irradiated receiving intracranial vehicle injection), irradiated (IRR) sham (receiving intracranial vehicle injection), EV-treated using intracranial surgeries (EV IC), and EV-treated using retro-orbital vein injections (EV RO). At 48 hours following irradiation, mice were sedated and maintained on 2.5% (v/v) isoflurane/oxygen and subjected to stereotaxic intrahippocampal EV-grafting surgery (EV IC group) or EV therapy delivered through circulation via the retro-orbital sinus (EV RO group). Intracranial injection was performed using a 33-gauge microsyringe at an injection rate of 0.25 μL/minute. Each hippocampus received two distinct injections of EVs per hemisphere in an injection volume of 2 μL (EV in sterile hibernation buffer) per site for a total of four injections (8 μL) and a total dose of 6.70×10^6 EVs per animal. Bilateral stereotactic coordinates from the bregma were anterior–posterior (AP): −1.94, mediolateral (ML): ±1.25, and dorsal–ventral (DV): −1.5 for the first site and AP: −2.60, ML: ±2.0, and DV: −1.5 for the second site. Control sham mice underwent intracranial procedures and received an equivalent injection of vehicle. To administer EVs via retro-orbital injection, mice were similarly sedated and 6.98×10^6 EVs in 50 μL of hibernation buffer were delivered into circulation.

miR-124 AAV cohort

Prior to surgery, miR-124 and miR-scramble (miR-Scr) were cloned into an AAV vector and efficacy of constructs was tested *in vitro* and then packaged into AAV9 Viral Particles (SignaGen Laboratories). AAV9 particles were purified and titrated via qPCR before suspending into sterile calcium- and magnesium-free PBS for injection. A single cohort of mice was randomly assigned to the following four experimental groups ($N = 12$ mice/group): 0 Gy + AAV9-miR-Scr, 0 Gy + AAV9-miR-124, 9 Gy + AAV9-miR-Scr, and 9 Gy + AAV9-miR-124. At 48 hours following irradiation, mice were sedated and maintained on 2.5% (v/v) isoflurane/oxygen and subjected to stereotaxic intrahippocampal AAV9 injections using a 33-gauge microsyringe at an injection rate of 0.25 μL/minute. Each hippocampus received two distinct injections per hemisphere in an injection volume of 1 μL viral particles per site for a total of four injections (4 μL) per animal. Bilateral stereotactic coordinates were the same as described above. The dose was approximately 3.5×10^{10} viral genomes (VG) per site and 1.4×10^{11} VGs per animal.

Cognitive testing

To determine the effect of both treatments on cognitive function after irradiation, mice were subjected to behavioral testing 5 weeks after irradiation. A cohort of EV-treated mice was tested at 6 months postirradiation as well. The 5-week EV cohort had 12 animals/group, and the 6-month EV cohort had 10 animals/group except the EV RO group, which had 14. The miR-124 cohort had 10–11 animals/group. Testing occurred over 5 weeks.

Open field testing

Three open field, spontaneous exploration tasks were used in the following order: novel place recognition (NPR), novel object recognition (NOR), and temporal order (TO). These tasks rely on intact hippocampus, medial prefrontal cortex (mPFC), and perirhinal cortex function. The NPR and NOR tasks evaluate the preference for novel location and object, respectively, in a test of episodic memory, while the TO task provides a measure of recency memory. Tasks were conducted as described previously (29) and all trials were scored by observers blind to the experimental groups to avoid bias. The average of those scores was used to determine performance, defined as a discrimination index (DI) and calculated as [(novel location exploration time/total exploration time) – (familiar location exploration time/total exploration time)] × 100.

Elevated plus maze

The elevated plus maze (EPM) provides a measure of anxiety-like behaviors in rodents that can be linked to the amygdala, by quantifying

Downloaded from cancerres.aacrjournals.org on December 28, 2020. © 2020 American Association for Cancer Research.

Published OnlineFirst August 19, 2020; DOI: 10.1158/0008-5472.CAN-20-1599

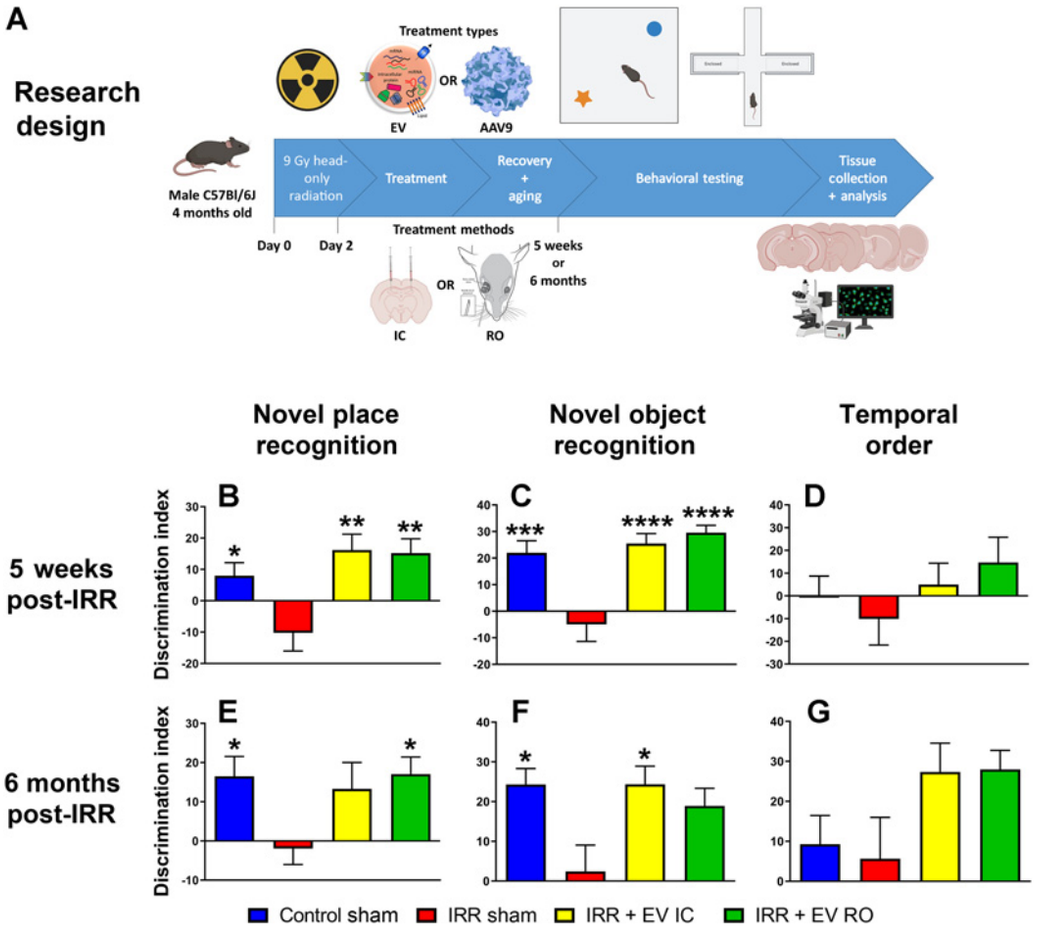

Figure 1.

Stem cell–derived EVs protect against RICD at 5 weeks and 6 months postirradiation. **A,** The experimental design for this studies is shown. Four-month-old male C57Bl/6J mice were immobilized and subjected to 9 Gy cranial irradiation using a ^{137}Cs γ irradiator at a dose rate of 2.07 Gy/minute. Two days later, mice were treated intracranially or retro-orbitally with EVs or miR-124 AAV9 particles. At 5 weeks and 6 months postirradiation, animals were administered spontaneous exploration tasks in the following order: NPR (**B** and **E**), NOR (**C** and **F**), and TO (**D** and **G**). The tendency to explore novelty (novel place or object) was calculated using the DI [(novel location exploration time/total exploration time) − (familiar location exploration time/total exploration time)] × 100. All data are presented as mean ± SEM ($N = 10$–14 mice per group). *, $P < 0.05$; **, $P < 0.01$; ***, $P < 0.001$; ****, $P < 0.0001$ compared with the IRR group; P values are derived from one-way ANOVA and Dunnett test for multiple comparisons.

the time spent and number of entries into the open versus closed arms of an elevated maze arranged as a symmetrical cross. The established anxiety-related indices for this test are the percentage of time spent in the open (uncovered) arm and the percentage of entries into the open arm. This test was not performed on the miR-124 cohort.

Light/dark box exploration test

The light/dark box (LDB) exploration test assesses anxiety in rodents. The light–dark test utilizes an arena (45 × 30 × 27 cm) where one-third of the box is a dark compartment and the other two-thirds is a well-lit compartment. The light and dark compartments were connected via a small opening (7.5 × 7.5 cm) that allowed the mice to freely move between the light and dark compartments. The light intensity measured in the light chamber was 900 lux and 4 lux in the dark chamber. Mice were placed at the center of the light compartment facing opposite to the small opening. The number of transitions between the compartments and the total time spent in the light compartment was recorded to quantify performance on this 10-minute test. Entry into a chamber was defined as all four paws crossing into the chamber. This test was not performed on the miR-124 cohort.

Fear extinction testing

To determine whether mice could learn and later extinguish conditioned fear responses, we performed a series of fear extinction (FE) assays modified to be reliant on hippocampal function (30). Testing occurred in a Behavioral Conditioning Chamber (17.5 × 17.5 × 18 cm, Coulbourn Instruments) with a steel slat floor (3.2 mm diameter slats and 8 mm spacing). The chamber was scented with a spray of 10% acetic acid in water. Initial fear conditioning (FC) was performed after mice were allowed to habituate in the chamber for 2 minutes. Three pairings of an auditory conditioned stimulus (16 kHz tone, 80 dB, lasting 120 seconds; CS) coterminating with a foot shock unconditioned stimulus (0.6 mA, 1 second; US) were presented at 2-minute intervals. On the following 3 days of extinction training, mice were presented with 20 non-US reinforced CS tones (16 kHz, 80 dB, lasting 120 seconds, at 5-second intervals) at 2-minute intervals. On

Downloaded from cancerres.aacrjournals.org on December 28, 2020. © 2020 American Association for Cancer Research.

Published OnlineFirst August 19, 2020; DOI: 10.1158/0008-5472.CAN-20-1599

the final day of fear testing, mice were presented with only three non-US reinforced CS tones (16 kHz, 80 dB, lasting 120 seconds, at 5-second intervals) at 2-minute intervals. Freezing behavior was recorded with a camera mounted above the chamber and scored by an automated measurement program (FreezeFrame, Coulbourn Instruments). This test was not performed on the miR-124 cohort.

IHC, confocal imaging, and analysis

After completion of behavioral testing, mice were deeply anesthetized using isoflurane and euthanized via intercardiac perfusion using 4% paraformaldehyde (Sigma) in 100 mmol/L PBS (100 mmol/L, pH 7.4; Gibco). Brains were cryoprotected using a sucrose gradient (10%–30%, Sigma) and sectioned coronally into 30-μm thick sections using a Cryostat (Microm HN 525 NX, Thermo Fisher Scientific). For each endpoint, 3–4 representative coronal brain sections from each of 4–6 animals per experimental group were selected at approximately 15-section intervals to encompass the rostro–caudal axis from the middle of the hippocampus and stored in PBS. Free floating sections were first rinsed in PBS, and then blocked for 30 minutes in 4% (w/v) BSA (Sigma) and 0.01% Triton (Sigma). For the immunofluorescence labeling of postsynaptic density 95 (PSD-95) and microglial activation marker, CD68, mouse anti–PSD-95 (Thermo Fisher Scientific; 1:1,000) and rat anti-mouse CD68 (1:500; AbD Serotec) primary antibodies were used with Alexa Fluor 594 secondary antibody (1:1,000). For immunofluorescence labeling of pan microglial marker, Iba1, rabbit anti-Iba1 (Wako Chemicals USA; 1:500) primary antibody was used with donkey anti-rabbit Alexa Fluor 488 secondary antibody (1:500). Tissues were then DAPI nuclear counterstained (1 μmol/L) and mounted using slow fade/antifade Mounting Medium (Life Technologies). Confocal analyses were carried out using multiple z stacks taken at 1-mm intervals through the 25–30 μm section using a Laser Scanning Confocal Microscope (Nikon Eclipse Ti-C2 interface). Individual z stacks were then analyzed using Nikon Elements AR Software (version 3.0). Images were deconvoluted using AutoQuant X3 and surface analysis was performed with Imaris version 9.2 (31).

EV labeling, tracking, and imaging

For *in vivo* tracking, EVs were labeled with the fluorescent dye PKH26 (Sigma-Aldrich) the day before transplantation. The EVs were then resuspended in diluent C and incubated with dye solution for 2 minutes with intermittent mixing as per the manufacturer's protocol. The dye was quenched with 1% BSA in water, and EVs were isolated through ultracentrifugation (28) and washed. EVs were administered to mice using stereotactic intrahippocampal injections or retro-orbital injections (as described above). At 48 hours postsurgery, animals were anesthetized, PFA perfused, and brains sectioned as described above. Following DAPI counterstain, sections were mounted onto slides and covered using antifade gold and cover slips. As before, imaging was done using a Nikon Eclipse Ti-C2 Laser Scanning Confocal Microscope. Images were deconvoluted using AutoQuant X3 and processed with Imaris version 9.2.

miRNA microarray

EVs were lysed using QIAzol and miRNA was isolated using the Qiagen miRNeasy Kit as per the manufacturer's protocol (Qiagen). Samples were analyzed for integrity and concentration (NanoDrop Technologies; 260/280 ratio > 1.6 and 260/230 ratio > 1.5), then processed and analyzed in duplicate on an miRNA Microarray Chip (Exiqon; Genomics Shared Resource at the University of Texas South Western Medical Center). Results were delivered as a spreadsheet of miRNA IDs and their associated expression values. Negative control probes were included for determination of significant hits. Another spreadsheet provided was filtered for probes that had duplicate measurements with less than 15% coefficient of variation and at least three SDs greater than the negative control probes.

Validation of EV miRNA

Validation of miRNA array data was performed using TaqMan Advanced miRNA Assays (Thermo Fisher Scientific). Total RNA was extracted from EVs using the RNA Miniprep Kit (Zymo Research Corp.). RNA template was then ligated to adaptors and preamplified using the TaqMan Advanced miRNA cDNA Synthesis Kit (Thermo Fisher Scientific) as per the manufacturer's protocol to obtain the cDNA template for classical qPCR using specific TaqMan Advanced miRNA Assays (Thermo Fisher Scientific), which are primers specific to the target miRNA. Duplicate reactions were set up in a 96-well plate with no-template controls (Milli-Q water instead of total RNA was used for cDNA synthesis process) included for each assay. Cycling was performed in the CFX96 (Bio-Rad Laboratories, Inc.). qPCR data were visualized and processed using CFX Manager Software (Bio-Rad Laboratories, Inc.).

Statistical analysis

Statistical data analyses were carried out using GraphPad Prism (v6). One-way ANOVA was used to assess significance between groups. When overall group effects were found to be statistically significant, a Dunnett multiple comparisons test was used to compare all other groups with the IRR or 9 Gy + miR-Scr group. All analyses considered a value of $P \leq 0.05$ to be statistically significant.

Results

Stem cell–derived EV treatment resolves RICD

Five weeks after irradiation and EV treatment, animals underwent behavioral testing (**Fig. 1**). The NPR test showed a significant overall group effect in DI between the groups ($F_{(3,44)} = 6.13$; $P = 0.0014$). The IRR group mean was −10.2%, which was lower than the control (mean = 7.99%), EV IC (mean = 16.2%), and EV RO (mean = 15.2%) groups (**Fig. 1B**). The difference in the mean DI was statistically significant between the IRR group and the control group ($P = 0.033$) and the EV-treated groups (EV IC: $P = 0.0014$ and EV RO: $P = 0.0021$). Similarly, a significant group effect was found for the NOR test ($F_{(3,43)} = 11.49$; $P < 0.0001$). The IRR group had a mean DI of −4.98%, whereas the control group (mean = 22.0%) and both of the EV treatment groups had higher mean DI values (EV IC: mean = 25.5% and EV RO: mean = 29.6%; **Fig. 1C**). For this test, all of the differences were statistically significant between the IRR group and the control ($P = 0.0004$), EV IC ($P < 0.0001$), and EV RO ($P < 0.0001$) groups. While no significant differences were observed in the TO test, the DI for the IRR group (mean = −10.1%) was lower than the control (mean = 0.228%) and both EV treatment groups (EV IC: mean = 4.98% and EV RO: mean = 14.7%; **Fig. 1D**). Total exploration times were not found to differ across the experimental cohorts, suggesting that treatment did not reduce locomotion or induce neophobic behavior to confound the findings (Supplementary Table S1).

To determine the persistence of the neurocognitive benefits of EV treatment, a second group of animals was administered the same spontaneous exploration tasks at 6 months after irradiation (**Fig. 1E–G**). The NPR test revealed a mean DI of −1.91% for the IRR group, whereas the DIs of the control (mean = 16.5%), EV IC (mean = 13.3%), and EV RO (mean = 17.0%) groups were higher. A significant

Downloaded from cancerres.aacrjournals.org on December 28, 2020. © 2020 American Association for Cancer Research.

Published OnlineFirst August 19, 2020; DOI: 10.1158/0008-5472.CAN-20-1599

overall group effect was found between mean DIs for this task ($F_{(3,39)} = 2.95$; $P = 0.044$). The mean differences in DI between the IRR group and the control and EV RO groups were statistically significant (**Fig. 1E**; $P = 0.048$ and $P = 0.028$, respectively). Similarly, the NOR test demonstrated mean DIs of 24.3%, 24.3%, and 18.9% for the control, EV IC, and EV RO groups, respectively, compared with 2.41% for the IRR group. A significant overall group effect for the mean DI between groups was also observed for NOR test ($F_{(3,40)} = 3.98$; $P = 0.014$). The mean DI differences between the control and EV RO groups and the IRR group were both statistically significant (**Fig. 1F**; $P = 0.014$ and $P = 0.013$, respectively), whereas the mean DI difference between IRR group and EV RO group was near the threshold for statistical significance ($P = 0.052$). Finally, the TO test did not reveal significant differences in DI between the control (mean = 9.29%) and IRR (mean = 5.66%) groups, although the EV-treated groups did exhibit higher preferences for novelty (EV IC: mean = 27.4% and EV RO: mean = 28.0%; **Fig. 1G**). The overall TO group effect for mean DIs did not reach significance ($F_{(3,34)} = 2.65$; $P = 0.065$). As with the 5-week tasks, total exploration times were not found to differ significantly between any of the groups, indicating that irradiation impaired episodic memory rather than disrupting locomotor activity (Supplementary Table S1).

To determine the effect of irradiation and EV treatments on anxiety-like behavior, the animals underwent testing on the EPM at both 5 weeks and 6 months postirradiation. While no differences were observed at the early timepoint (Supplementary Fig. S1A), at 6 months posttreatment, anxiety-like behavior was increased in the IRR group (mean = 0.714) compared with the control group (mean = 0.571; $P = 0.058$), but to a lesser extent when compared with the EV-treated groups (EV IC: mean = 0.649 and EV RO: mean = 0.676; Supplementary Fig. S1B). As a second measure of anxiety-like behavior, mice were also subjected to the LDB exploration test. As with the EPM, the LDB test measures an animal's unconditioned response, where an anxious mouse will spend more time in the dark compartment of the arena than in the light compartment, and less time moving freely between the two compartments. No significant group effects were observed at either 5 weeks or 6 months posttreatment (Supplementary Fig. S1C and S1D).

In the final behavioral assessment, mice were subjected to a hippocampal-dependent FC and FE task. During the conditioning phase of the task, all of the groups learned to associate the tone (conditioned stimulus) to the subsequent foot shock (unconditioned stimulus) as measured by freezing behavior (i.e., not moving; Supplementary Fig. S1E and S1G; T_1–T_3). For the 5-week cohort, the mean level of freezing at T_3 was more than 40% for all groups and no significant differences were found between groups. Similarly, the 5-week cohort exhibited no significant differences between groups during the subsequent 3-day extinction training period, as measured by a gradual decrease in the percent time spent freezing (Supplementary Fig. S1E). On the final extinction test day, however, there was a trend for a higher level of freezing in the IRR group (mean = 15.0%) compared with the control (mean = 8.63%) and the EV-treated groups (EV IC: mean = 6.59% and EV RO: mean = 10.2%), although this did not reach statistical significance (Supplementary Fig. S1F). At the 6-month timepoint, all groups were subjected to the same testing paradigms and were found to be conditioned to a level of freezing of 30% at T_3. At this later time, neither the extinction training sessions nor final extinction test showed significant differences among cohorts (Supplementary Fig. S1G and S1H).

Tracking EVs following intracranial transplantation and retro-orbital injection

Red fluorescent (PKH26) dye–labeled EVs were used to determine whether EVs migrate equally to various regions of the brain following distinct administration routes. In the intracranial transplanted mice, at 48 hours after injection, EVs were found in the dentate gyrus (DG) and CA1 regions of the hippocampus adjacent to the transplantation sites (**Fig. 2A** and **C**). In the brain of the retro-orbital injected mice also, fluorescence EVs were present in the DG and CA1 regions (**Fig. 2B** and **D**). We have previously shown that there were no obvious differences in the distribution of EVs through hippocampus, subventricular zone, and mPFC regions delivered by either route (32).

Stem cell–derived EV treatment reduces microglial activation in the irradiated hippocampus

Following behavior testing, CD68, a marker for activated microglia, was evaluated to assess the impact of EV treatments on neuroinflammation (**Fig. 3**). Representative images show the DG region of the hippocampus in brain sections from the 5-week testing cohort (**Fig. 3A–D**). The number of CD68-positive cells for the IRR group, as quantified by total fluorescence volume per hippocampal section (mean = 2.68×10^4 μm^3), was significantly greater than that of the control group (mean = 1.68×10^4 μm^3) and the EV IC group (mean = 1.72×10^4 μm^3), with P values of 0.034 and 0.048, respectively (**Fig. 3E**). For the EV RO group, there was a trend toward reduced

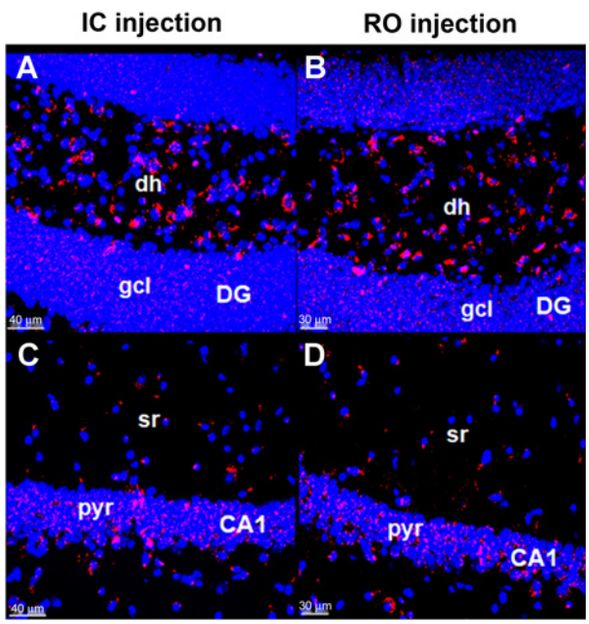

Figure 2.
Stem cell–derived EVs tracked to the host hippocampus following retro-orbital or intracranial injections. Fluorescently labeled hNSC-derived EVs were transplanted using stereotactic intracranial or retro-orbital injections. Brain tissue was fixed at 48 hours postsurgery and brain sections were imaged using confocal microscopy. Analysis suggests that intracranially injected EVs (**A** and **C**) and retro-orbitally injected EVs (**B** and **D**) were similarly effective in targeting the DG (**A** and **B**) and CA1 (**C** and **D**) regions of the hippocampus. Red, fluorescently labeled EV membranes; blue, DAPI nuclear counterstain. Scale bars, 30 μm (retro-orbital method) and 40 μm (intracranial method). dh, dentate hilus; gcl, granule cell layer; sr, striatum radiatum; pyr, pyramidal cell layer.

Downloaded from cancerres.aacrjournals.org on December 28, 2020. © 2020 American Association for Cancer Research.

Published OnlineFirst August 19, 2020; DOI: 10.1158/0008-5472.CAN-20-1599

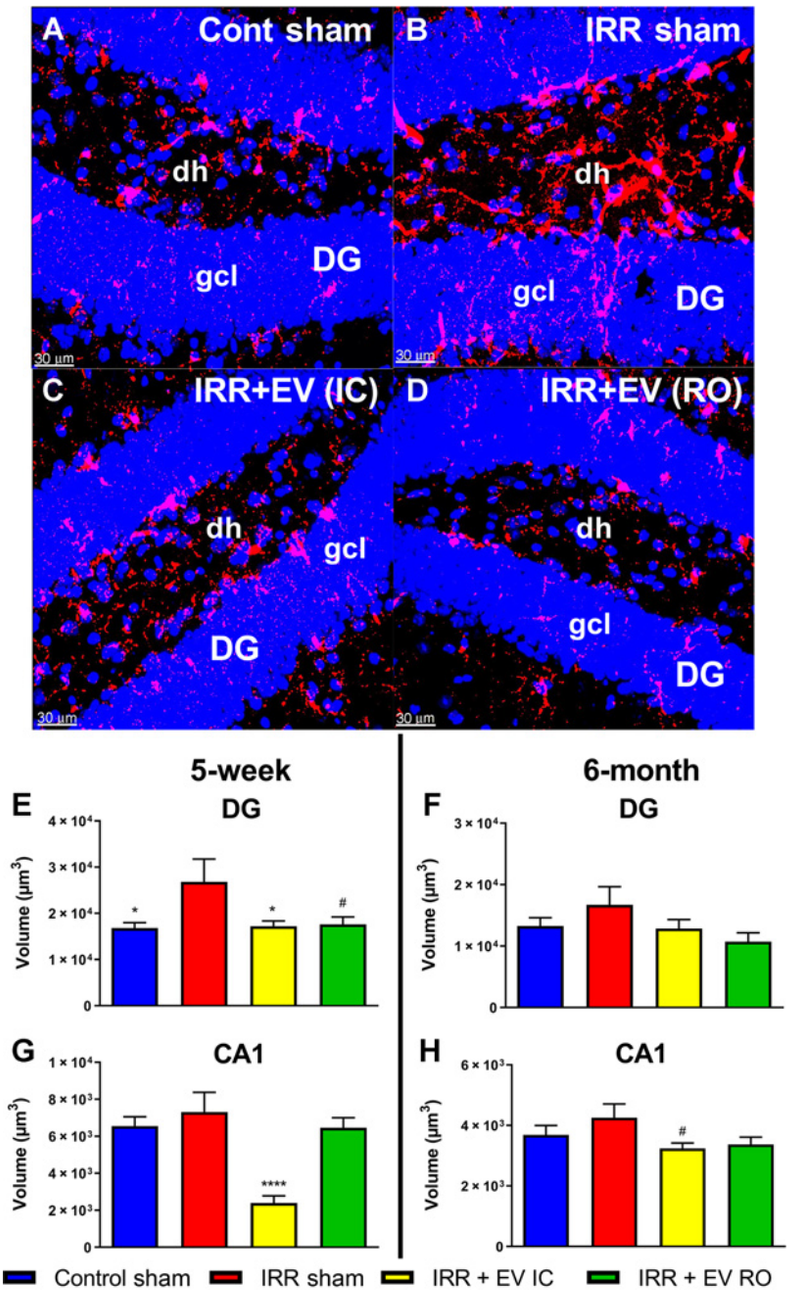

Figure 3.

Stem cell–derived EV treatment reduces neuroinflammation in the hippocampus following irradiation. Representative images of $CD68^+$ activated microglia are shown from the DG region of the hippocampus in all four groups for the 5-week behavioral testing cohort. Relative to controls (**A**), the DG region of the hippocampus from irradiated mice show elevated levels of CD68 (**B**). EV treatment reduces CD68 levels in the irradiated brain [**C** and **D**; intracranial (IC) and retroorbital (RO), respectively]. Aggregate data from image processing with Imaris show an increased volume of staining in the irradiated group compared with the control and EV-treated groups in the DG region in both the 5-week (**E**) and 6-month (**F**) cohorts. The same analysis showed similar trends in the CA1 region of the hippocampus in both the 5-week (**G**) and 6-month (**H**) cohorts. All data are presented as mean ± SEM ($N = 4$–6 mice per group). #, $P = 0.061$; *, $P < 0.05$; ****, $P < 0.0001$ compared with the IRR group; P values are derived from ANOVA and Dunnett multiple comparisons test (all other groups compared with IRR group). Red, CD68; blue, DAPI nuclear counterstain. Scale bars, 30 μm. dh, dentate hilus; gcl, granule cell layer.

CD68 levels (1.76×10^4 μm^3; $P = 0.061$). The other hippocampal regions and timepoints showed similar trends for a higher volume of staining in the IRR group as compared with the control and EV-treated groups (**Fig. 3F–H**).

PSD-95 is an excitatory-associated synaptic protein responsible for recruiting receptors and other proteins to the synaptic cleft. Changes in protein levels of PSD-95 have been shown to be altered following irradiation in a manner that may disrupt neurotransmission and contribute to cognitive dysfunction. However, evaluation of PSD-95 protein levels at both timepoints postirradiation revealed no significant radiation effects (Supplementary Fig. S2).

miRNA microarray analysis reveals miR-124 as potential therapeutic EV cargo

To investigate functional components of EV, total RNA was extracted from the hNSC-derived EVs and analyzed using a targeted human miRNA array (Supplementary Table S2). By cross-referencing the array data with the literature, candidate EV miRNAs implicated in learning, memory, neurogenesis, neurotransmission, synaptogenesis, and neuroinflammation were identified. These target miRNAs included miR-134-3p, miR-125b-5p, miR-124-3p, and miR-125a-5p (**Fig. 4A**). Of these candidates, all except miR-134-3p were confirmed to be present in EV RNA samples using TaqMan advanced miRNA assays (**Fig. 4B–D**), providing three candidate miRNAs (miR-125b-

Downloaded from cancerres.aacrjournals.org on December 28, 2020. © 2020 American Association for Cancer Research.

Published OnlineFirst August 19, 2020; DOI: 10.1158/0008-5472.CAN-20-1599

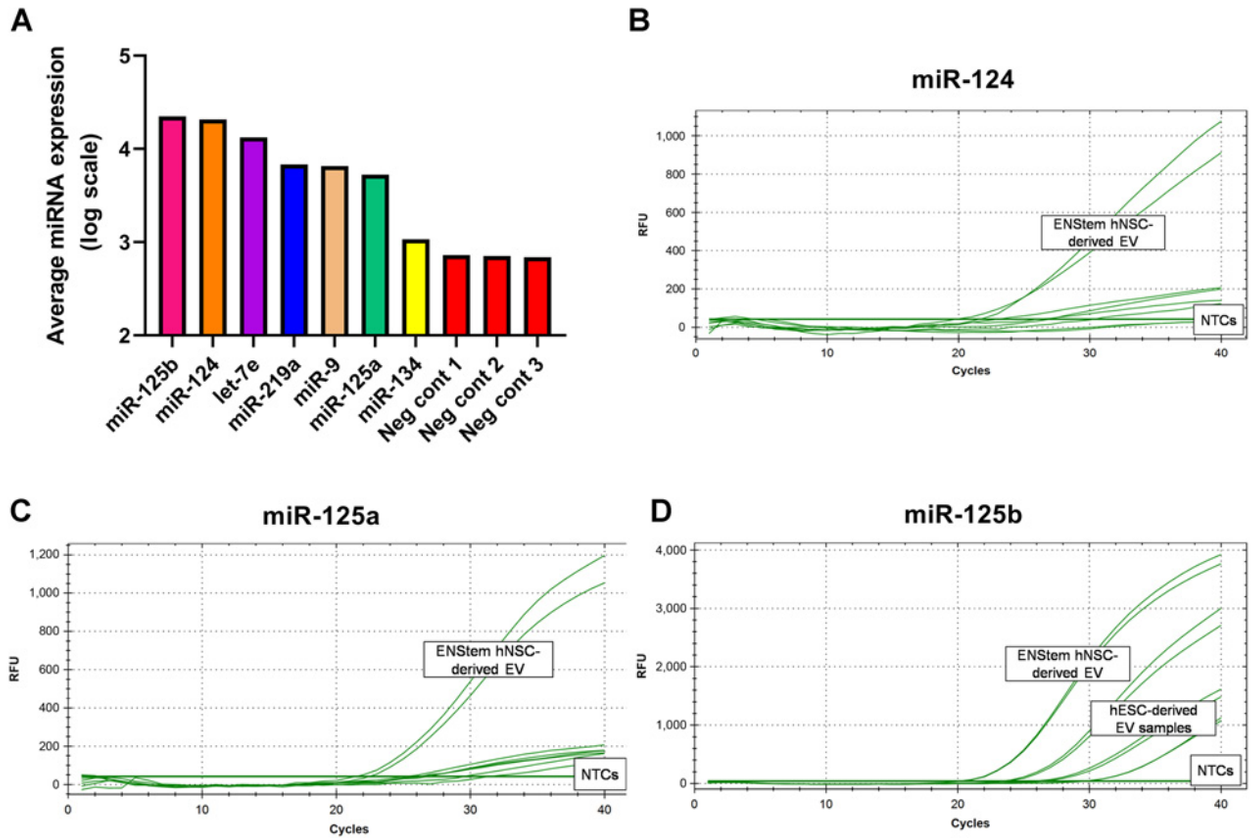

Figure 4.

hNSC-derived EVs contain candidate miRNA that may mitigate RICD. Total RNA extracted from therapeutic EVs was analyzed by miRNA microarray. **A,** Select examples from array data included four miRNAs with significant literature suggesting roles for them in synaptic function, dendrite outgrowth, and reduction in neuroinflammation. Of these four, three miRNAs (hsa-miR-124-3p, hsa-miR-125a-5p, and hsa-miR-125b-5p) could be validated using TaqMan advanced miRNA assays (**B–D**).

5p, miR-124-3p, and miR-125a-5p) for follow-up studies. On the basis of abundance of literature (33–42) in support of a role for miR-124-3p in reducing neuroinflammation, miR-124-3p was chosen for further study.

Hippocampal miR-124 overexpression can mitigate RICD

To determine whether hsa-miR-124-3p (miR-124) was sufficient to mitigate RICD in wild-type mice, the miR-124 sequence was cloned into an overexpression AAV vector and the construct was packaged into AAV9 particles (SignaGen; **Fig. 5A**). As with EV treatments, wild-type male mice were cranially irradiated with the same 9 Gy dose of γ-rays and received stereotaxic injections 48 hours later with the miR-124 AAV9 construct or a scrambled control. The miR-124–treated mice underwent behavioral testing at 5 weeks post-irradiation (**Fig. 5B–D**). The NPR test revealed a significant overall group effect in DI between groups ($F_{(3,38)} = 2.91$; $P = 0.0468$). The 9 Gy + miR-Scr group's mean DI was 4.87%, which was lower than the mean DI of the 0 Gy + miR-124 (mean = 21.5%; $P = 0.055$) and 9 Gy + miR-124 (mean = 16.2%; $P = 0.265$) groups. In this instance, only a small difference in mean DI was observed between the 9 Gy + miR-Scr group and the 0 Gy + miR-Scr group (mean = 5.23%; **Fig. 5B**). Similarly, a significant group effect was found for the NOR test ($F_{(3,38)} = 3.51$; $P = 0.0244$). The 9 Gy + miR-Scr group had a mean DI of 3.03%, whereas the 9 Gy + miR-124 group (mean = 28.8%; $P = 0.0072$) had significantly higher mean DI values. The DI values for the 0 Gy groups were also higher, although not so significantly (0 Gy + miR-Scr: mean = 16.0%; $P = 0.244$ and 0 Gy + miR-124: mean = 17.6%; $P = 0.181$; **Fig. 5C**). The group effect in the case of the TO test did not reach significance ($F_{(3,30)} = 2.73$; $P = 0.0615$). In a result similar to the NOR test, the DI for the 9 Gy + miR-Scr group (mean = −1.69%) was observed to be significantly lower than the 9 Gy + miR-124 (mean = 29.4%; $P = 0.0474$) group and lower than both 0 Gy groups (0 Gy + miR-Scr: mean = 18.6%; $P = 0.215$ and 0 Gy + miR-124: mean = 25.9%; $P = 0.0724$; **Fig. 5D**). Total exploration times were found to be significantly different between the 0 Gy + miR-Scr and 0 Gy + miR-124 groups for the NOR test as well as the 0 Gy + miR-124 and 9 Gy + miR-Scr groups for the TO test. The rest of the total exploration times were not found to differ across the experimental cohorts for these tests, suggesting that treatment-induced locomotor changes did not confound our findings (Supplementary Table S3).

The spread of AAV9 particles and expression of the GFP reporter gene was confirmed experimentally (**Fig. 6**). Expression of the transgene construct was not limited to the area proximal to the injection sites in the hippocampus, but rather spread to the cortex (**Fig. 6A**) and

Downloaded from cancerres.aacrjournals.org on December 28, 2020. © 2020 American Association for Cancer Research.

Published OnlineFirst August 19, 2020; DOI: 10.1158/0008-5472.CAN-20-1599

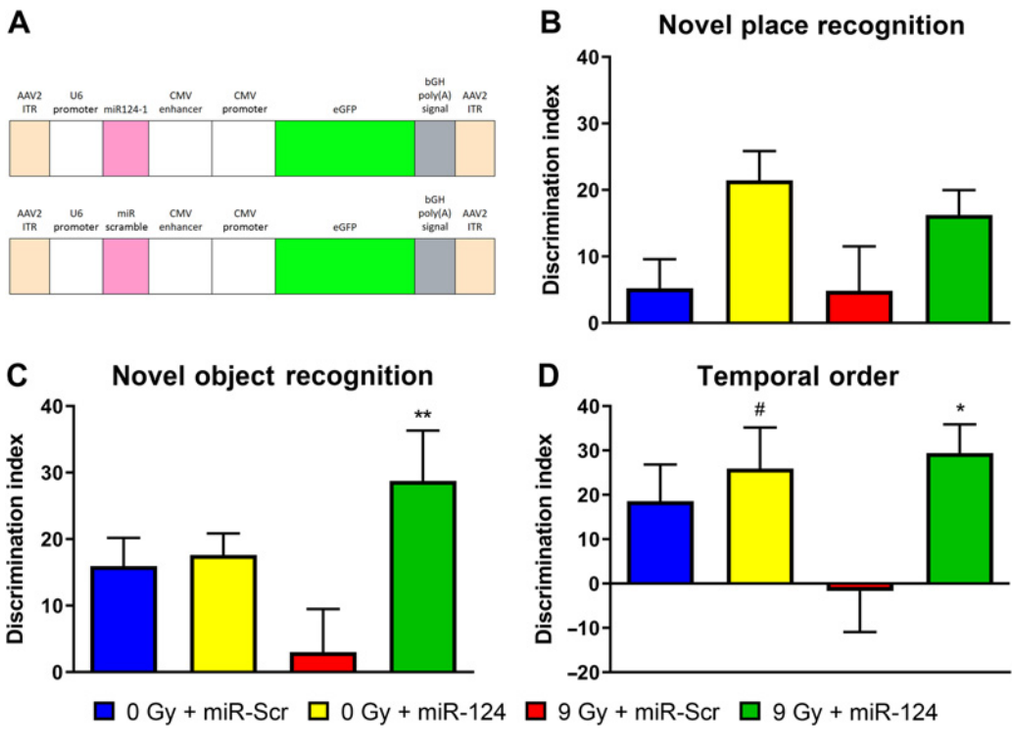

Figure 5.

miR-124 overexpression *in vivo* shows functional mitigation of RICD. To determine whether miR-124 was sufficient to mitigate RICD in wild-type mice, the miRNA sequence was cloned into a vector designed to overexpress miR-124 and the construct packaged into AAV9 particles. **A,** The vector map (designed by SignaGen) shows that miR-124 expression is driven by the U6 promoter and eGFP expression is driven by the CMV enhancer and promoter. These transgenes are flanked by AAV2 inverted terminal repeats (ITR) for efficient propagation of the AAV genome. Mice received stereotaxic intracranial injections of AAV9 particles containing this vector 2 days postirradiation. At 5 weeks postirradiation, animals were administered spontaneous exploration tasks in the following order: NPR (**B**), NOR (**C**), and TO (**D**). Tendency to explore novelty (novel place or object) was calculated using the DI [(novel location exploration time/total exploration time) − (familiar location exploration time/total exploration time)] × 100. All data are presented as mean ± SEM ($N = 10$–11 mice per group). #, $P = 0.0724$; *, $P < 0.05$; **, $P < 0.01$ compared with the IRR group. *P* values are derived from one-way ANOVA and Dunnett test for multiple comparisons (all other groups compared with the 9 Gy + miR-Scr group).

corpus callosum (**Fig. 6B**), as well. On the basis of morphology, GFP expression was detected in both neuronal and glial cell types (**Fig. 6C** and **D**).

miR-124 overexpression reduced microglial activation

Similar to the EV-treated cohort, CD68 immunoreactivity was evaluated following behavioral testing to assess the impact of miR-124 overexpression on neuroinflammation (**Fig. 7**). Representative images show the impact of miR-124 overexpression on both the total number of microglia assessed using the Iba1 marker (**Fig. 7A** and **B**) and the amount of microglial activation indicated by the CD68 marker (**Fig. 7C** and **D**) in the irradiated hippocampus. Aggregate data from image processing using Imaris show a decrease in $Iba1^+$ cells in the hippocampus of in the 9 Gy + miR-Scr group compared with all other groups (**Fig. 7E**). The volume of CD68 staining was measured for both DG and CA1 regions of the hippocampus, combined, and adjusted for the average number of $Iba1^+$ hippocampal microglia in each group (**Fig. 7F**). A significant overall group effect was observed for the difference in staining between groups ($F_{(3,82)} = 10.7$; $P < 0.0001$). The adjusted CD68 immunoreactivity value for the 9 Gy + miR-Scr group (mean = 239) was significantly greater than that of the 0 Gy + miR-Scr group (mean = 152; $P = 0.0045$) and the miR-124–overexpressing groups (0 Gy + miR-124: mean = 140; $P = 0.0009$ and 9 Gy + miR-124: mean = 91.1; $P < 0.0001$). In sum, data showed that miR-124 overexpression resulted in functionally equivalent effects as EV treatments, where reductions in neuroinflammation coincided with an amelioration of RICD.

Discussion

Ionizing radiation has been and will likely remain a powerful tool in the fight against cancer. The major limitation to the efficacy of radiotherapy is the resultant dose-dependent normal tissue toxicity. Multiple dose delivery strategies have emerged in an attempt to mitigate downstream damage (7–10, 14, 15) or avoid this complication using either precise tumor targeting (43–45) or ultrahigh dose rate (46–48). While hNSC-derived EVs have been used to effectively mitigate normal tissue toxicity in nude rats (14, 15), current findings are the first example of using EVs for this purpose in immunocompetent animals. Moreover, these data demonstrate the efficacy of a mildly invasive and translationally feasible route of administration. While replicating past stem cell transplantation studies using EV therapy in an athymic nude rat model was a logical first step, the real advantages of this strategy were borne out in this study.

Current findings show, for the first time, that an intravenous (retro-orbital) injection of hNSC-derived EVs to cranially irradiated wild-type mice was able to significantly mitigate RICD and accompanying neuroinflammation. The beneficial effects of the EV therapy were

Downloaded from cancerres.aacrjournals.org on December 28, 2020. © 2020 American Association for Cancer Research.

Published OnlineFirst August 19, 2020; DOI: 10.1158/0008-5472.CAN-20-1599

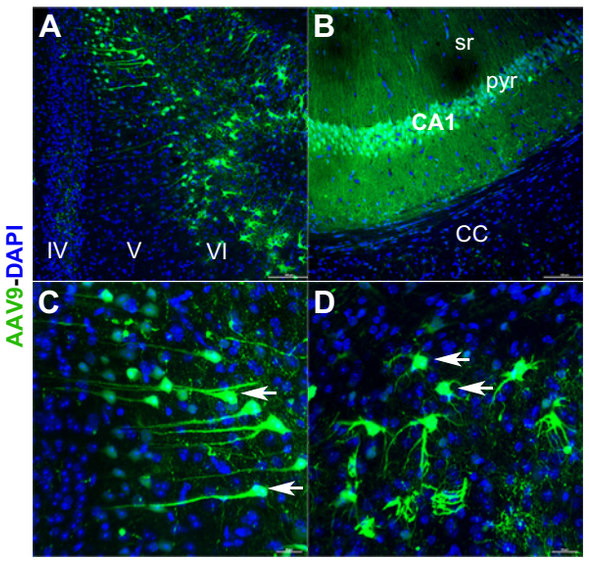

Figure 6.

Reporter gene confirmation and tracking of AAV9-miR-124 *in vivo*. The AAV9 vector designed to express either intact or scrambled miR-124 carried the eGFP reporter gene to enable construct visualization *in vivo*. After completion of behavior (8–10 weeks postsurgery), coronal brain sections were imaged for the presence of eGFP signal. Widespread expression of vector (green) was found in the cortex (layers IV–VI; **A**), corpus callosum (CC), and hippocampus (CA1; pyr, pyramidal layer; and sr, stratum radiatum; **B**). Vector expression was evident in the cells resembling neuronal (**C**, arrows) and glial morphologies (**D**, arrows). Scale bars, 100 μm (**A** and **B**) and 20 μm (**C** and **D**).

consistent for both the known (intrahippocampal; ref. 14) and the novel (retro-orbital) methods of delivery as well as at the short (5 weeks) and long (6 months) postirradiation times. Furthermore, we were able to identify a potential mechanism of action for EV therapy. We hypothesized and then tested the ability of a specific miRNA, miR-124, to mitigate RICD and neuroinflammation *in vivo*. Importantly, overexpression of this specific miRNA, just one known component of the bioactive EV cargo, was sufficient to impart significant neuroprotective phenotypes.

Cognitive testing results from a battery of spontaneous exploration tasks demonstrated conclusively the onset and persistence of RICD, specifically affecting the hippocampus, perirhinal cortex, and mPFC regions of the brain, serious complications mitigated by EV treatment. Interestingly, just a single dose of EVs (or *in vivo* overexpression of miR-124) administered 48 hours postirradiation was efficacious in mitigating RICD. While repeated treatments were not tested, this translationally feasible approach facilitates implementation of serial administration schedules that could provide further neuroprotective benefits at the cognitive, cellular, and molecular levels especially at more protracted times. While multiple systemic injections of EV would be relatively simple and straightforward, the behavioral data at both 5 weeks and 6 months postirradiation suggest that a single dose is sufficient to maintain long-term intact hippocampal, perirhinal cortex, and mPFC function.

Collectively, data showed the hNSC-derived EVs were equally able to colocalize to the brain via local (intracranial) or systemic (retro-orbital) routes of administration. Furthermore, these results confirmed prior studies suggesting that EVs could cross the blood–brain barrier and interact with specific cellular subtypes in the brain (24, 25). Intracranial tracking of fluorescence EVs revealed no obvious differences in distribution, which was widespread throughout the hippocampal subfields (**Fig. 2**). Coalescence of EVs surrounding target cells was revealed by the presence of larger fluorescence aggregates 48 hours after injection, likely representing multiple fusion events between EVs of unknown functional significance. Additional studies are required to determine optimal dosing and whether molecular modifications could be undertaken to target EVs to specific cell types for select phenotypic modulation.

While multiple mechanisms are likely responsible for the beneficial effects of EV treatments on the irradiated brain, their ability to modulate inflammatory processes provides a plausible explanation. Neuroinflammation has been shown to play a significant role in progressive neurodegenerative conditions such as Alzheimer disease, Parkinson disease, and multiple sclerosis (49). Moreover, our group has previously shown an increase in activated microglia following irradiation that was abrogated by EV treatment (14, 15). Given the robust attenuation of microglial activation by EV treatments, the identification of miR-124 as an EV cargo component, and the wealth of literature on miR-124 reducing neuroinflammation in similar models (33, 40, 42), further studies were then focused on evaluating the functional relevance of miR-124.

AAV9 constructs designed to drive the overexpression of miR-124 were then injected directly into the mouse hippocampus to critically test whether this could resolve, in part, RICD and associated normal tissue pathology in the brain. Intrahippocampal injections were selected for these proof-of-principle studies to target miR-124 overexpression to a selected region of the brain and to avoid systemic dilution of the viral particles. Tracking of eGFP reporter expression (**Fig. 6**) indicated that AAV9 particles were able to spread from the hippocampal injection sites and drive transgene expression in neurons and glial cells. Data showed that miR-124 overexpression was able to mitigate RICD in a similar, albeit less efficacious fashion than EV treatments. Many explanations could account for this, as it is extremely likely that the neuroprotective benefits of EVs involve more than one miRNA or other EV cargo. Another reason could be related to the amount of time it takes to reach maximal expression of the AAV construct, generally achieved by 2 weeks (50). Thus, optimal expression, bioavailability, and proximity of EV treatment to irradiation are all factors that could clearly impact the therapeutic benefits of miR-124. While further studies to inhibit miR-124 via antagomirs or miR-sponges may provide further mechanistic insight, miR-124 is ubiquitous in CNS tissues (51), pointing to the potential confounding off-target effects of such approaches.

This study represents an exciting development in the field of normal tissue protection following radiation injury. While we focused on miR-124 overexpression, hNSC-derived EVs contained other candidate molecular cargo. Inhibition of miR-125a has been shown to decrease levels of PSD-95 in dendrites (52), and miR-125b has been shown to regulate synaptic structure and function (53). Furthermore, combinations of miRNAs could be more effective than individual ones, such that a "miR cocktail" could be loaded into cell culture–derived EVs, liposomes (54), or artificially engineered EVs (55, 56). Amelioration of RICD might also be achieved from EVs derived from other normal brain cell types such as mature neurons, astrocytes, and microglia, or even mesenchymal stem cell–derived EVs that have been shown to reduce inflammation in other models (57, 58). Systemic efficacy could also be optimized by engineering various EV types to contain a transmembrane protein and/or moiety for targeting purposes (42). As with the previous studies (7–10, 14, 15, 31, 48), this study was performed using tumor-free animals to study the biological mechanisms and

Downloaded from cancerres.aacrjournals.org on December 28, 2020. © 2020 American Association for Cancer Research.

Published OnlineFirst August 19, 2020; DOI: 10.1158/0008-5472.CAN-20-1599

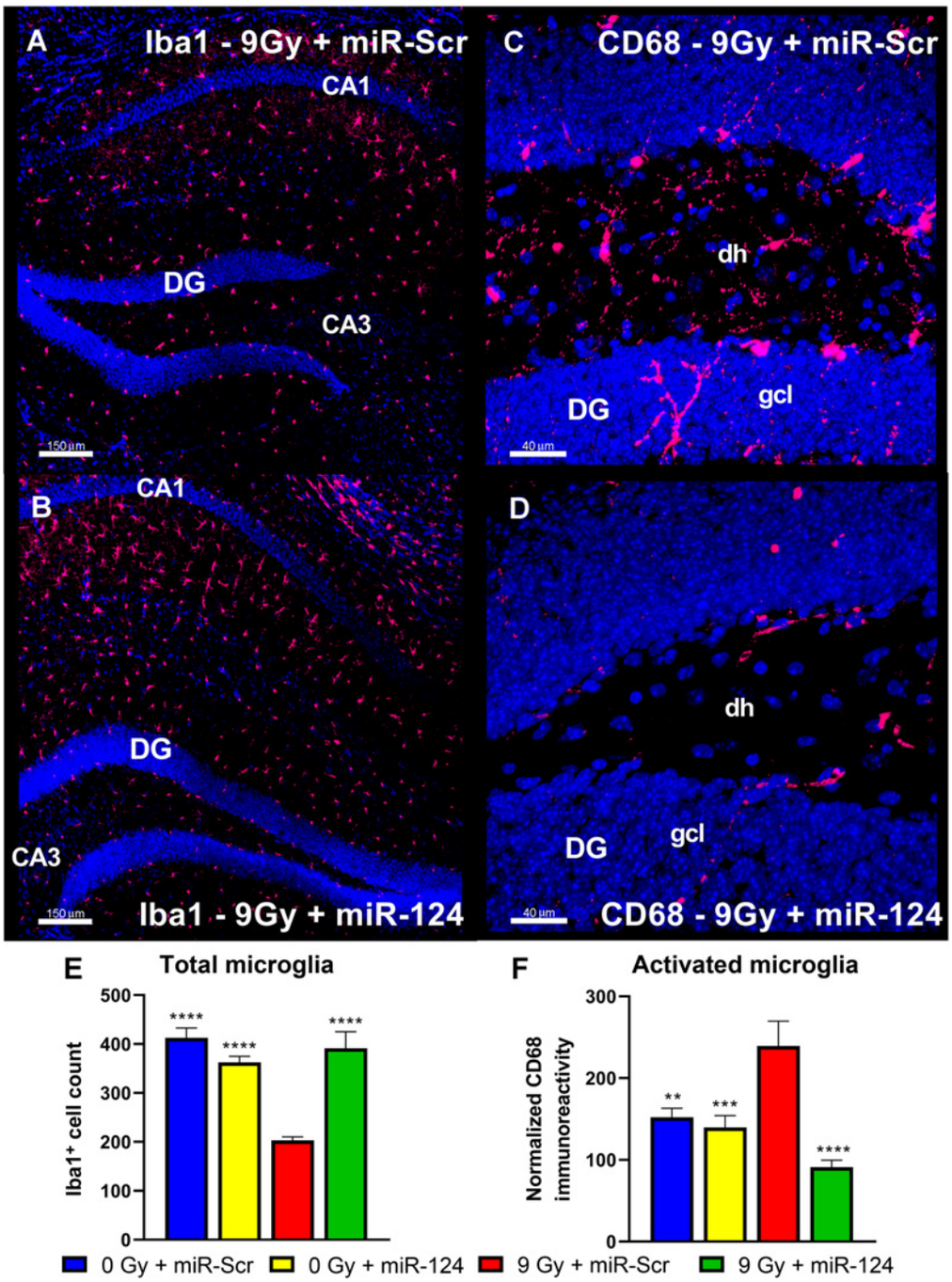

Figure 7.

miR-124 overexpression *in vivo* following cranial irradiation reduces neuroinflammation in the hippocampus. Representative images of Iba1$^+$ microglia- and CD68$^+$-activated microglia IHC are shown from the hippocampus and DG, respectively, for the 9 Gy + miR-Scr and the 9 Gy + miR-124 groups of the miR-124 cohort. Relative to miR-124–overexpressing group (**B**), the mice in the 9 Gy + miR-Scr group showed decreased numbers of Iba1$^+$ cells in hippocampal subfields (**A**). miR-124 overexpression (**D**) resulted in a relative decrease in the CD68$^+$ immunoreactivity in the DG region when compared with the 9 Gy + miR-Scr group (**C**). Volumetric analysis of Iba1-adjusted CD68 immunoreactivity (**E** and **F**) show elevation in the irradiated group compared with the control and miR-124–overexpressing groups in the hippocampus. All data are presented as mean ± SEM ($N = 4$ mice per group). **, $P < 0.01$; ***, $P < 0.001$; ****, $P < 0.0001$ compared with the IRR group; P values are derived from ANOVA and Dunnett multiple comparisons test. Red, Iba1; red, CD68; blue, DAPI nuclear counterstain. Scale bars, 150 µm (**A** and **B**) and 40 µm (**C** and **D**). dh, dentate hilus; gcl, granule cell layer.

Downloaded from cancerres.aacrjournals.org on December 28, 2020. © 2020 American Association for Cancer Research.

Published OnlineFirst August 19, 2020; DOI: 10.1158/0008-5472.CAN-20-1599

physiologic effect in the absence of confounding disease. Before any clinical application involving radiotherapy is to be used in the context of cancer treatment, EV–tumor cell interactions would have to be investigated for lack of tumor promotion and changes to treatment efficacy. Furthermore, a single dose of whole brain radiotherapy was used in current studies to follow-up on the significant body of work from our laboratory implementing such a dosing scheme. While previous studies (59, 60) have shown that fractionated irradiation causes RICD, follow-up studies aimed at determining how EVs might mitigate RICD after dose fractionation and in female mice are clearly warranted.

Over the years, our group, among others, has not included grafted controls (either stem cells or EVs) because such transplantation procedures used to treat a variety of pathologies in different rodent models were not found to functionally affect the intact normal brain (14, 18, 20, 42, 61). Importantly, past work from us using stem cells (62), and from others using EVs (63, 64), in which grafted controls were included, found that every single functional or molecular endpoint was statistically indistinguishable between the control, control + stem cell, or control + EV groups. Further rationale for excluding controls treated with EVs alone is that inclusion of such cohorts is clinically irrelevant.

Here, we highlight the benefits of EV treatments, which have certain advantages over stem cell–based approaches for resolving normal tissue complications (11–13). The ability to impart neuroprotective benefits to the irradiated brain without the need for invasive surgical procedures, and immune suppression or risk of teratoma formation bode well for future clinical translation. Moreover, we were able to identify some of the beneficial bioactive miRNA cargo in EVs, which suggests similar approaches and/or combinations of miRNA will hold additional benefits. Any approach capable of minimizing dose-limiting toxicities to a target tissue or organ is poised to provide opportunities for dose escalation and enhanced radiocurability for the eventual benefit of those afflicted with cancer worldwide.

Disclosure of Potential Conflicts of Interest

No potential conflicts of interest were disclosed.

Authors' Contributions

R.J. Leavitt: Conceptualization, formal analysis, investigation, methodology, writing-original draft, writing-review and editing. **M.M. Acharya:** Formal analysis, supervision, investigation, writing-review and editing. **J.E. Baulch:** Conceptualization, formal analysis, funding acquisition, investigation, writing-original draft, writing-review and editing. **C.L. Limoli:** Conceptualization, formal analysis, funding acquisition, writing-original draft, writing-review and editing.

Acknowledgments

The authors thank Erich Giedzinski, Maria Angulo, Lauren Apodaca, Ning Ru, Liping Yu, and Sana Jayaswal for expert technical assistance. The authors would also like to thank Dr. Michael Story and his group at UTSW for providing the microarray data. The authors also thank UC Irvine Professors Drs. Kim Green and Matthew Blurton-Jones for expert advice concerning the miR-124 overexpression project. Special thanks to Darryl Leja of the NHGRI for use of his illustration of the retro-orbital injection used in **Fig. 1**. This work was supported by NINDS grant R01 NS074388 (to C.L. Limoli), the UCI Research Seed Funding Program (to J.E. Baulch), and California Institute for Regenerative Medicine DISC1–10079 (to J.E. Baulch).

The costs of publication of this article were defrayed in part by the payment of page charges. This article must therefore be hereby marked *advertisement* in accordance with 18 U.S.C. Section 1734 solely to indicate this fact.

Received May 13, 2020; revised July 8, 2020; accepted August 7, 2020; published first August 19, 2020.

References

1. Stupp R, Hegi ME, Mason WP, van den Bent MJ, Taphoorn MJ, Janzer RC, et al. Effects of radiotherapy with concomitant and adjuvant temozolomide versus radiotherapy alone on survival in glioblastoma in a randomised phase III study: 5-year analysis of the EORTC-NCIC trial. Lancet Oncol 2009;10:459–66.
2. Lee YW, Cho HJ, Lee WH, Sonntag WE. Whole brain radiation-induced cognitive impairment: pathophysiological mechanisms and therapeutic targets. Biomol Ther 2012;20:357–70.
3. Meyers CA. Neurocognitive dysfunction in cancer patients. Oncology 2000;14:75–9.
4. Roman DD, Sperduto PW. Neuropsychological effects of cranial radiation: current knowledge and future directions. Int J Radiat Oncol Biol Phys 1995;31:983–98.
5. Abayomi OK. Pathogenesis of irradiation-induced cognitive dysfunction. Acta Oncol 1996;35:659–63.
6. Anderson VA, Godber T, Smibert E, Weiskop S, Ekert H. Cognitive and academic outcome following cranial irradiation and chemotherapy in children: a longitudinal study. Br J Cancer 2000;82:255–62.
7. Acharya MM, Christie LA, Lan ML, Giedzinski E, Fike JR, Rosi S, et al. Human neural stem cell transplantation ameliorates radiation-induced cognitive dysfunction. Cancer Res 2011;71:4834–45.
8. Acharya MM, Martirosian V, Christie LA, Limoli CL. Long-term cognitive effects of human stem cell transplantation in the irradiated brain. Int J Radiat Biol 2014;90:816–20.
9. Acharya MM, Martirosian V, Christie LA, Riparip L, Strnadel J, Parihar VK, et al. Defining the optimal window for cranial transplantation of human induced pluripotent stem cell-derived cells to ameliorate radiation-induced cognitive impairment. Stem Cells Transl Med 2015;4:74–83.
10. Acharya MM, Rosi S, Jopson T, Limoli CL. Human neural stem cell transplantation provides long-term restoration of neuronal plasticity in the irradiated hippocampus. Cell Transplant 2015;24:691–702.
11. Bradley JA, Bolton EM, Pedersen RA. Stem cell medicine encounters the immune system. Nat Rev Immunol 2002;2:859–71.
12. Blum B, Benvenisty N. The tumorigenicity of human embryonic stem cells. Adv Cancer Res 2008;100:133–58.
13. Gutierrez-Aranda I, Ramos-Mejia V, Bueno C, Munoz-Lopez M, Real PJ, Macia A, et al. Human induced pluripotent stem cells develop teratoma more efficiently and faster than human embryonic stem cells regardless the site of injection. Stem Cells 2010;28:1568–70.
14. Baulch JE, Acharya MM, Allen BD, Ru N, Chmielewski NN, Martirosian V, et al. Cranial grafting of stem cell-derived microvesicles improves cognition and reduces neuropathology in the irradiated brain. Proc Natl Acad Sci U S A 2016;113:4836–41.
15. Smith SM, Giedzinski E, Angulo MC, Lui T, Lu C, Park AL, et al. Functional equivalence of stem cell and stem cell-derived extracellular vesicle transplantation to repair the irradiated brain. Stem Cells Transl Med 2020;9:93–105.
16. Xin H, Li Y, Buller B, Katakowski M, Zhang Y, Wang X, et al. Exosome-mediated transfer of miR-133b from multipotent mesenchymal stromal cells to neural cells contributes to neurite outgrowth. Stem Cells 2012;30:1556–64.
17. Xin H, Li Y, Cui Y, Yang JJ, Zhang ZG, Chopp M. Systemic administration of exosomes released from mesenchymal stromal cells promote functional recovery and neurovascular plasticity after stroke in rats. J Cereb Blood Flow Metab 2013;33:1711–5.
18. Xin H, Li Y, Liu Z, Wang X, Shang X, Cui Y, et al. MiR-133b promotes neural plasticity and functional recovery after treatment of stroke with multipotent mesenchymal stromal cells in rats via transfer of exosome-enriched extracellular particles. Stem Cells 2013;31:2737–46.
19. Zhang Y, Chopp M, Meng Y, Katakowski M, Xin H, Mahmood A, et al. Effect of exosomes derived from multipluripotent mesenchymal stromal cells on functional recovery and neurovascular plasticity in rats after traumatic brain injury. J Neurosurg 2015;122:856–67.

Downloaded from cancerres.aacrjournals.org on December 28, 2020. © 2020 American Association for Cancer Research.

Published OnlineFirst August 19, 2020; DOI: 10.1158/0008-5472.CAN-20-1599

20. Zhang Y, Chopp M, Zhang ZG, Katakowski M, Xin H, Qu C, et al. Systemic administration of cell-free exosomes generated by human bone marrow derived mesenchymal stem cells cultured under 2D and 3D conditions improves functional recovery in rats after traumatic brain injury. Neurochem Int 2017; 111:69–81.
21. Gangoda L, Boukouris S, Liem M, Kalra H, Mathivanan S. Extracellular vesicles including exosomes are mediators of signal transduction: are they protective or pathogenic? Proteomics 2015;15:260–71.
22. Cocucci E, Meldolesi J. Ectosomes and exosomes: shedding the confusion between extracellular vesicles. Trends Cell Biol 2015;25:364–72.
23. Zhang J, Li S, Li L, Li M, Guo C, Yao J, et al. Exosome and exosomal microRNA: trafficking, sorting, and function. Genomics Proteomics Bioinformatics 2015;13: 17–24.
24. Kalani A, Tyagi A, Tyagi N. Exosomes: mediators of neurodegeneration, neuroprotection and therapeutics. Mol Neurobiol 2014;49:590–600.
25. Alvarez-Erviti L, Seow Y, Yin H, Betts C, Lakhal S, Wood MJ. Delivery of siRNA to the mouse brain by systemic injection of targeted exosomes. Nat Biotechnol 2011;29:341–5.
26. Zhu X, Badawi M, Pomeroy S, Sutaria DS, Xie Z, Baek A, et al. Comprehensive toxicity and immunogenicity studies reveal minimal effects in mice following sustained dosing of extracellular vesicles derived from HEK293T cells. J Extracell Vesicles 2017;6:1324730.
27. Acharya MM, Lan ML, Kan VH, Patel NH, Giedzinski E, Tseng BP, et al. Consequences of ionizing radiation-induced damage in human neural stem cells. Free Radic Biol Med 2010;49:1846–55.
28. Thery C, Amigorena S, Raposo G, Clayton A. Isolation and characterization of exosomes from cell culture supernatants and biological fluids. Curr Protoc Cell Biol 2006;Chapter 3:Unit 3.22.
29. Acharya MM, Baulch JE, Klein PM, Baddour AAD, Apodaca LA, Kramar EA, et al. New concerns for neurocognitive function during deep space exposures to chronic, low dose-rate, neutron radiation. eNeuro 2019;6. DOI: 10.1523/ENEURO.0094-19.2019.
30. Chang CH, Knapska E, Orsini CA, Rabinak CA, Zimmerman JM, Maren S. Fear extinction in rodents. Curr Protoc Neurosci 2009;Chapter 8:Unit8 23.
31. Acharya MM, Green KN, Allen BD, Najafi AR, Syage A, Minasyan H, et al. Elimination of microglia improves cognitive function following cranial irradiation. Sci Rep 2016;6:31545.
32. Ioannides P, Giedzinski E, Limoli CL. Evaluating different routes of extracellular vesicle administration for cranial therapies. J Cancer Metastasis Treat 2020;6:15.
33. Yu A, Zhang T, Duan H, Pan Y, Zhang X, Yang G, et al. MiR-124 contributes to M2 polarization of microglia and confers brain inflammatory protection via the C/EBP-alpha pathway in intracerebral hemorrhage. Immunol Lett 2017;182:1–11.
34. Huang S, Ge X, Yu J, Han Z, Yin Z, Li Y, et al. Increased miR-124-3p in microglial exosomes following traumatic brain injury inhibits neuronal inflammation and contributes to neurite outgrowth via their transfer into neurons. FASEB J 2018; 32:512–28.
35. Sun Y, Li Q, Gui H, Xu DP, Yang YL, Su DF, et al. MicroRNA-124 mediates the cholinergic anti-inflammatory action through inhibiting the production of pro-inflammatory cytokines. Cell Res 2013;23:1270–83.
36. Yao L, Ye Y, Mao H, Lu F, He X, Lu G, et al. MicroRNA-124 regulates the expression of MEKK3 in the inflammatory pathogenesis of Parkinson's disease. J Neuroinflammation 2018;15:13.
37. Geng L, Liu W, Chen Y. miR-124-3p attenuates MPP(+)-induced neuronal injury by targeting STAT3 in SH-SY5Y cells. Exp Biol Med 2017;242:1757–64.
38. Periyasamy P, Thangaraj A, Guo ML, Hu G, Callen S, Buch S. Epigenetic promoter DNA methylation of miR-124 promotes HIV-1 Tat-mediated microglial activation via MECP2-STAT3 axis. J Neurosci 2018;38:5367–83.
39. Periyasamy P, Liao K, Kook YH, Niu F, Callen SE, Guo ML, et al. Cocaine-mediated downregulation of miR-124 activates microglia by targeting KLF4 and TLR4 signaling. Mol Neurobiol 2018;55:3196–210.
40. Yang Y, Ye Y, Kong C, Su X, Zhang X, Bai W, et al. MiR-124 enriched exosomes promoted the M2 polarization of microglia and enhanced hippocampus neurogenesis after traumatic brain injury by inhibiting TLR4 pathway. Neurochem Res 2019;44:811–28.
41. Ponomarev ED, Veremeyko T, Barteneva N, Krichevsky AM, Weiner HL. MicroRNA-124 promotes microglia quiescence and suppresses EAE by deactivating macrophages via the C/EBP-alpha-PU.1 pathway. Nat Med 2011;17:64–70.
42. Yang J, Zhang X, Chen X, Wang L, Yang G. Exosome mediated delivery of miR-124 promotes neurogenesis after ischemia. Mol Ther Nucleic Acids 2017;7:278–87.
43. Nwokedi EC, DiBiase SJ, Jabbour S, Herman J, Amin P, Chin LS. Gamma knife stereotactic radiosurgery for patients with glioblastoma multiforme. Neurosurgery 2002;50:41–6.
44. Hsieh PC, Chandler JP, Bhangoo S, Panagiotopoulos K, Kalapurakal JA, Marymont MH, et al. Adjuvant gamma knife stereotactic radiosurgery at the time of tumor progression potentially improves survival for patients with glioblastoma multiforme. Neurosurgery 2005;57:684–92.
45. Crowley RW, Pouratian N, Sheehan JP. Gamma knife surgery for glioblastoma multiforme. Neurosurg Focus 2006;20:E17.
46. Favaudon V, Caplier L, Monceau V, Pouzoulet F, Sayarath M, Fouillade C, et al. Ultrahigh dose-rate FLASH irradiation increases the differential response between normal and tumor tissue in mice. Sci Transl Med 2014; 6:245ra93.
47. Montay-Gruel P, Petersson K, Jaccard M, Boivin G, Germond JF, Petit B, et al. Irradiation in a flash: unique sparing of memory in mice after whole brain irradiation with dose rates above 100 Gy/s. Radiother Oncol 2017;124: 365–9.
48. Montay-Gruel P, Acharya MM, Petersson K, Alikhani L, Yakkala C, Allen BD, et al. Long-term neurocognitive benefits of FLASH radiotherapy driven by reduced reactive oxygen species. Proc Natl Acad Sci U S A 2019;116: 10943–51.
49. Kempuraj D, Thangavel R, Natteru PA, Selvakumar GP, Saeed D, Zahoor H, et al. Neuroinflammation induces neurodegeneration. J Neurol Neurosurg Spine 2016;1:1003.
50. Klein RL, Dayton RD, Tatom JB, Diaczynsky CG, Salvatore MF. Tau expression levels from various adeno-associated virus vector serotypes produce graded neurodegenerative disease states. Eur J Neurosci 2008;27:1615–25.
51. Lagos-Quintana M, Rauhut R, Yalcin A, Meyer J, Lendeckel W, Tuschl T. Identification of tissue-specific microRNAs from mouse. Curr Biol 2002;12: 735–9.
52. Muddashetty RS, Nalavadi VC, Gross C, Yao X, Xing L, Laur O, et al. Reversible inhibition of PSD-95 mRNA translation by miR-125a, FMRP phosphorylation, and mGluR signaling. Mol Cell 2011;42:673–88.
53. Edbauer D, Neilson JR, Foster KA, Wang CF, Seeburg DP, Batterton MN, et al. Regulation of synaptic structure and function by FMRP-associated microRNAs miR-125b and miR-132. Neuron 2010;65:373–84.
54. Malam Y, Loizidou M, Seifalian AM. Liposomes and nanoparticles: nanosized vehicles for drug delivery in cancer. Trends Pharmacol Sci 2009;30:592–9.
55. Antimisiaris SG, Mourtas S, Marazioti A. Exosomes and exosome-inspired vesicles for targeted drug delivery. Pharmaceutics 2018;10:218.
56. Wang J, Li W, Lu Z, Zhang L, Hu Y, Li Q, et al. The use of RGD-engineered exosomes for enhanced targeting ability and synergistic therapy toward angiogenesis. Nanoscale 2017;9:15598–605.
57. Timmers L, Lim SK, Arslan F, Armstrong JS, Hoefer IE, Doevendans PA, et al. Reduction of myocardial infarct size by human mesenchymal stem cell conditioned medium. Stem Cell Res 2007;1:129–37.
58. Lee RH, Pulin AA, Seo MJ, Kota DJ, Ylostalo J, Larson BL, et al. Intravenous hMSCs improve myocardial infarction in mice because cells embolized in lung are activated to secrete the anti-inflammatory protein TSG-6. Cell Stem Cell 2009;5:54–63.
59. Allen BD, Acharya MM, Lu C, Giedzinski E, Chmielewski NN, Quach D, et al. Remediation of radiation-induced cognitive dysfunction through oral administration of the neuroprotective compound NSI-189. Radiat Res 2018; 189:345–53.
60. Dey D, Parihar VK, Szabo GG, Klein PM, Tran J, Moayyad J, et al. Neurological impairments in mice subjected to irradiation and chemotherapy. Radiat Res 2020;193:407–24.
61. Long Q, Upadhya D, Hattiangady B, Kim DK, An SY, Shuai B, et al. Intranasal MSC-derived A1-exosomes ease inflammation, and prevent abnormal neurogenesis and memory dysfunction after status epilepticus. Proc Natl Acad Sci U S A 2017;114:E3536–E45.
62. Acharya MM, Christie LA, Lan ML, Donovan PJ, Cotman CW, Fike JR, et al. Rescue of radiation-induced cognitive impairment through cranial transplantation of human embryonic stem cells. Proc Natl Acad Sci U S A 2009; 106:19150–5.
63. Kalani A, Chaturvedi P, Kamat PK, Maldonado C, Bauer P, Joshua IG, et al. Curcumin-loaded embryonic stem cell exosomes restored neurovascular unit following ischemia-reperfusion injury. Int J Biochem Cell Biol 2016;79:360–9.
64. Drommelschmidt K, Serdar M, Bendix I, Herz J, Bertling F, Prager S, et al. Mesenchymal stem cell-derived extracellular vesicles ameliorate inflammation-induced preterm brain injury. Brain Behav Immun 2017;60:220–32.

Downloaded from cancerres.aacrjournals.org on December 28, 2020. © 2020 American Association for Cancer Research.

Published OnlineFirst August 19, 2020; DOI: 10.1158/0008-5472.CAN-20-1599

Cancer Research
The Journal of Cancer Research (1916–1930) | The American Journal of Cancer (1931–1940)

AACR American Association for Cancer Research

Extracellular Vesicle–Derived miR-124 Resolves Radiation-Induced Brain Injury

Ron J. Leavitt, Munjal M. Acharya, Janet E. Baulch, et al.

Cancer Res 2020;80:4266-4277. Published OnlineFirst August 19, 2020.

Updated version	Access the most recent version of this article at: doi:10.1158/0008-5472.CAN-20-1599
Supplementary Material	Access the most recent supplemental material at: http://cancerres.aacrjournals.org/content/suppl/2020/08/19/0008-5472.CAN-20-1599.DC1

Cited articles	This article cites 61 articles, 6 of which you can access for free at: http://cancerres.aacrjournals.org/content/80/19/4266.full#ref-list-1

E-mail alerts	Sign up to receive free email-alerts related to this article or journal.
Reprints and Subscriptions	To order reprints of this article or to subscribe to the journal, contact the AACR Publications Department at pubs@aacr.org.
Permissions	To request permission to re-use all or part of this article, use this link http://cancerres.aacrjournals.org/content/80/19/4266. Click on "Request Permissions" which will take you to the Copyright Clearance Center's (CCC) Rightslink site.

Downloaded from cancerres.aacrjournals.org on December 28, 2020. © 2020 American Association for Cancer Research.